O–D bond dissociation from the 3*s* state of deuterated hydroxymethyl radical (CH_2OD)

Lin Feng, Andrey V. Demyanenko, and Hanna Reisler[a)]
Department of Chemistry, University of Southern California, Los Angeles, California 90089-0482

(Received 31 January 2003; accepted 11 March 2003)

The photodissociation of the deuterated hydroxymethyl radical CH_2OD is investigated on the lowest excited state, the 3*s* Rydberg state, in the wavelength region 365–318 nm where the D atom is the only significant product. The translational energy distribution and kinetic energy-dependent anisotropy parameter of the D channel are determined by the core-sampling time-of-flight technique at 352.5 nm. The negative recoil anisotropy parameter $\beta_{\text{eff}}=-0.7\pm0.1$ is consistent with the perpendicular nature of the transition from the ground state. The fraction of the available energy partitioned into the translational degree of freedom is 0.69. Ground state products CH_2O ($1\,^1A_1$) + D constitute the main photodissociation channel, and no significant H product is detected at these wavelengths. Comparison with the conical intersection calculations of Hoffman and Yarkony suggests that O–D bond rupture involves crossing from the 3*s* potential energy surface to a repulsive region of the ground state surface at a large O–D bond distance. Isomerization of CH_2OD to CH_2DO is not competitive with the fast O–D dissociation. © *2003 American Institute of Physics.* [DOI: 10.1063/1.1571526]

I. INTRODUCTION

Studies of photodissociation dynamics of free radicals are important in atmospheric and environmental chemistry,[1] but experimental results are scarce, because of difficulties in developing intense and contaminant-free sources. The open-shell electronic structure of free radicals often gives rise to low-lying valence electronic states. In addition, because radicals usually have low ionization potentials, they have Rydberg states lying in the same energy region as their lowest valence states. The interactions among these states complicate the interpretation of their spectroscopy and photodissociation dynamics.

The hydroxymethyl radical has attracted considerable attention, because of its potential importance in fuel combustion and atmospheric chemistry. It is known that the reactions of $O(^1D)$ with methane and ethane,[2,3] and reactions of Cl atoms and OH radicals with methanol yield the hydroxymethyl radical as a significant product.[4–7] The photochemistry of CH_2OH is interesting from another perspective: it has been predicted theoretically that CH_2OH requires $\sim16\,000\ \text{cm}^{-1}$ to surmount the barrier to $H+CH_2O$ ($^1A_1$) on the ground state,[8,9] while experiment has established that the corresponding barrier for CH_3O decomposition is $\sim11\,000\ \text{cm}^{-1}$ relative to the energy of CH_2OH.[10,11] Since less energy is required to dissociate CH_2OH via the CH_3O route, the height of the isomerization barrier (calculated at $\sim14\,000\ \text{cm}^{-1}$)[9] is of importance.

According to *ab initio* calculations, the lowest excited electronic states of the CH_2OH radical have a predominant Rydberg character,[5,12,13] and are characterized, in turn, as the $3s$, $3p_x$, $3p_y$, and $3p_z$ states. The UV absorption spectrum includes a broad and structureless band that starts at ~385 nm and extends to below 351 nm. It has recently been assigned to $1\,^2A'(3s)\leftarrow1\,^2A''$ excitation.[14] Vibrational structure is observed, however, in the transitions from the ground state to the $3p_x$ and $3p_z$ states, but no rotational features can be resloved.[4,5,14–16] The photodissociation of CH_2OD via the origin band of the $3p_z$ state [~5.09 eV (244 nm)] was studied before,[15–17] and D products were detected as major fragments. The final dissociation step from this state was proposed to evolve on the ground state surface.

The Rydberg $3s$, $3p_x$, $3p_y$, and $3p_z$ states (at 3.22, 4.34, 4.89, and 5.09 eV, respectively[5,13–15]) have planar geometries resembling the ground state ion, and they are also close in energy. Thus, in the dissociation from the $3p_z$ state the Franck–Condon factors are more favorable for inter-Rydberg couplings than coupling directly to the ground state, and multiple surface crossings are expected en route to the dissociative state. Therefore, in order to elucidate the dissociation mechanism, it is desirable to promote the radical directly to the lowest excited 3*s* state. At photon energies that access this state, multiple photodissociation channels[16] are thermochemically allowed:

$$CH_2OD\rightarrow CH_2O(^1A_1)+D,\quad \Delta H=1.32\pm0.07\ \text{eV}, \tag{I}$$

$$CH_2OD\rightarrow CH_2DO\rightarrow CH_2O+D\quad \Delta H=1.32\pm0.07\ \text{eV},$$
$$\rightarrow CHDO+H,\quad \Delta H=1.32\pm0.07\ \text{eV}, \tag{II}$$

$$CH_2OD\rightarrow H_2+COD\rightarrow H_2+CO+D\quad \Delta H=1.31\pm0.02\ \text{eV}, \tag{III}$$

$$\rightarrow HD+HCO\rightarrow HD+CO+H$$
$$\Delta H=1.28\pm0.02\ \text{eV}, \tag{IV}$$

$$\rightarrow HCOD+H,\quad \Delta H\approx3.54\ \text{eV}. \tag{V}$$

a)Electronic mail: reisler@usc.edu

In this paper, we describe the photodissociation from the $3s$ state in the region 365–318 nm. Since the results in this wavelength region are similar, we only report detailed studies at 352.5 nm (3.51 eV). At this energy, reaction (V) is closed and the radicals can only predissociate via the ground electronic state. By minimizing the number of open channels and potential energy surfaces (PES) involved in the dissociation via the $3s$ state, the mechanism of the dissociation can be simplified. Comparison between our experimental results and the theoretical calculations of Hoffman and Yarkony[18] suggests that the intersection seam of the $3s$ and ground states is located in the repulsive region, of the O–D coordinate, disfavoring isomerization.

II. EXPERIMENT

A. Radical production

The experiments are performed in a pulsed molecular beam as described before.[14–16] A mixture of 4% CH_3OD (Aldrich, used without further purification), ~1% Cl_2 (Air gas, 99.5%), and He is first prepared in a glass bulb at a total pressure of 2.0 atm. The mixture is then expanded through a pulsed valve with an attached quartz tube (~4 mm long, 1 mm inner diameter). The photodissociation of Cl_2 to Cl atoms is achieved by 355 nm radiation from a Nd:YAG laser (Spectra Physics, GCR-11; 8 mJ, focused by a 30 cm f.l. cylindrical lens) directed onto the quartz tube. CH_2OD radicals are produced by the reaction $CH_3OD + Cl \rightarrow CH_2OD + HCl$. By controlling the position of the 355 nm laser beam along the quartz tube, the rapid consecutive reaction $Cl + CH_2OD \rightarrow CH_2O + DCl$ is suppressed.[15] After the supersonic expansion, the radicals are skimmed (Beam Dynamics, 1.51 mm diameter) and introduced into the detection chamber. Hydroxymethyl radicals with densities of 10^{12}–10^{13} cm^{-3} are produced with a rotational temperature of ~10 K, as estimated from the $1+1'$ two-color resonance enhanced multiphoton ionization (REMPI) spectrum via the $3p_z$ state.[15] No vibrational "hot bands" are observed.[5,15]

B. Photodissociation and product detection

UV radiation (the pump) from a Nd:YAG laser-pumped OPO (Continuum, PL8000/Sunlite/FX-1; 0.5 mJ; 40 cm f.l. lens) is used to excite the $3s$ state. H and D product detection is achieved by $1+1'$ two-color (~121.6+365 nm) REMPI via the L-α transition. The doubled output (~365 nm, 2 mJ) of a Nd:YAG pumped dye laser system (Continuum, PL8010/ND6000, LDS 751) is focused into a mixture of Kr:Ar (120:490 Torr) in a tripling cell. A MgF_2 lens (75 mm f.l. lens) then refocuses the tripled 121.6 nm radiation (the probe) into the chamber. The pump and probe laser beams are counterpropagating, and cross the molecular beam at right angle. The time delay between them is 1.0 ± 1.0 ns.

Time-of-flight (TOF) distributions of the photofragments are recorded by the core-sampling technique combined with REMPI detection of the products. This method has been described in detail elsewhere.[16] In brief, the core-sampling arrangement consists of a two-stage ion acceleration region, an 18 cm field-free drift region, and a 4 mm-diam aperture installed in front of a multichannel plate detector (MCP, Galileo, 25 mm). The aperture is mounted on a linear motion feedthrough (MDC, BLM-133-4) to allow alternation between total ion collection and core sampling. In core sampling, the speed distribution is obtained directly because the small aperture rejects ions having off-axis velocities.[19–22] The ion detector is positioned parallel to the plane defined by the molecular and the laser beams. TOF spectra of the products are recorded at pump polarizations parallel ($\parallel$) and perpendicular ($\perp$) to the TOF axis. The alternation of the polarization is accomplished by controlling the time delay between the triggering of the pump laser pulse and a Photoelastic Modulator (PEM-80, HINDS International, Inc.). This procedure makes it possible to switch polarization of the pump without an alignment change—an improvement over our previous arrangement.[16] The TOF distribution is converted to a differential cross section by the transformation procedure described before.[16] In our experiment, the space focusing condition is achieved by adjusting the voltages applied to the two electrode plates of the spectrometer until the TOF of CH_2OD^+ is insensitive to a shift of the pump laser beam along the TOF axis within the extraction region. This condition depends only on the ratio of the voltages applied to the two electrode plates. Under space-focusing conditions, the smaller the extraction field, the better the resolution. However there is a trade-off between temporal resolution and signal-to-noise ratio, and in our experiment, the applied voltage on the extractor plate is adjusted for optimal operation, giving energy resolution $\Delta E/E \sim 1\%$. Photodissociation of acetylene at 121.6 nm is used to calibrate and test our system.[22]

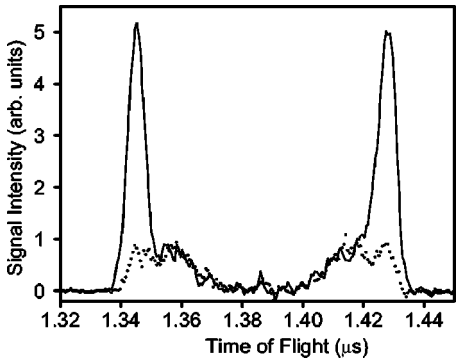

FIG. 1. D fragment time-of-flight spectra from CH_2OD photodissociation at 352.5 nm. The polarization of the photolysis laser beam is kept parallel (dotted line) or perpendicular (solid line) to the TOF axis. The signals have been normalized to the laser power and the number of laser shots.

III. RESULTS AND DISCUSSION

Figure 1 depicts D-atom TOF spectra obtained in the photodissociation of CH_2OD at 352.5 nm. The dotted (solid) D signal curve corresponds to UV pump radiation polarization parallel (perpendicular) to the TOF axis. These signals depend on both the 355 nm and the pump laser beams. The background signals taken by either blocking the pump or the 355 nm laser beam are subtracted in these spectra.

Product translational energy and angular distributions in the photodissociation can be expressed as

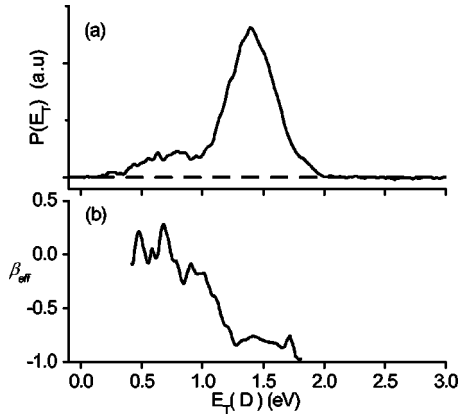

FIG. 2. (a) D photofragment translational energy distribution and (b) E_T dependence of the effective anisotropy parameter, β_{eff}, of CH_2OD at 352.5 nm.

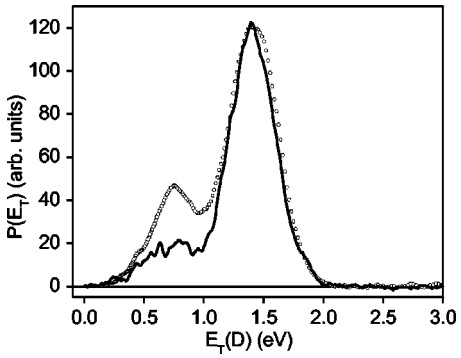

FIG. 3. D photofragment translational energy distributions of CH_2OD under different experiment conditions. The solid curve corresponds to the 355 nm laser beam positioned at the far end of the quartz tube, while the circles depict results when the laser beam is close to the pulsed valve aperture.

$$P(E_T,\theta)=\frac{1}{4\pi}P(E_T)[1+\beta_{\text{eff}}(E_T)P_2(\cos\theta)], \tag{1}$$

where β_{eff} is the effective anisotropy parameter ($-1\leqslant\beta_{\text{eff}}\leqslant 2$; its value can be affected by molecular geometry and dissociation lifetime), θ is the angle between the electric vector of the polarized pump radiation and the recoil velocity vector of the D-atom product, $P_2(\cos\theta)$ is the second Legendre polynomial, and $P(E_T)$ is the angle-integrated translational energy distribution of the detected photofragment. For dissociation to two fragments, the total center-of-mass (c.m.) translational energy distribution is computed from

$$E_{T,\text{c.m.}}=E_T\left(\frac{M}{M-m}\right), \tag{2}$$

where M is the mass of parent molecular and m is the detected fragment mass. The energy-dependent anisotropy parameter $\beta_{\text{eff}}(E_T)$ is calculated by using

$$\beta_{\text{eff}}(E_T)=\frac{P_{\parallel}(E_T)-P_{\perp}(E_T)}{\frac{1}{2}P_{\parallel}(E_T)+P_{\perp}(E_T)}, \tag{3}$$

where $P_{\parallel}(E_T)$ and $P_{\perp}(E_T)$ are the detected D product energy distributions obtained in the core-sampling experiment with parallel ($\parallel$) and perpendicular ($\perp$) polarizations relative to the TOF axis, respectively. In Fig. 2, both the translational energy distribution and the E_T-dependent anisotropy parameter of the D fragment are presented.

The D photofragment translational energy distribution exhibits two distinct peaks with markedly different β_{eff} values. The high energy component that extends toward ~2 eV has an almost constant β_{eff} value of -0.7 ± 0.1, while the low energy peak at ~0.8 eV is isotropic ($\beta_{\text{eff}}\approx 0$). The change in $\beta_{\text{eff}}(E_T)$ suggests that there are two sources of D signal. Since the results reported here are based exclusively on monitoring photofragments and the $3s\leftarrow 1\,^2A''$ transition does not exhibit a vibrational structure, it is essential to determine whether the precursor of all the observed D products is CH_2OD. In our experiments, radical production is confirmed by observing the narrow (~20 cm^{-1}) CH_2OD^+ obtained via the origin band of the $3p_z\leftarrow 1\,^2A''$ transition, obtained by 1+1 REMPI at ~244 nm.[5,15] For this transition, the CH_2OD and D REMPI signals exhibit the same distinct vibrational structure.[16] With this method we also confirm that vibrational ''hot bands'' are not present in the REMPI spectra. Possible contributions from methanol photodissociation can be accounted for by subtracting the background obtained with the 355 nm radiation turned off.

The dependence of the TOF spectra on experimental conditions was investigated in a controlled way. We found that the product signals depended linearly on pump energy. We observed, however, that the relative ratio of the high to low energy D peaks in Fig. 2 depended on the position of the Cl_2 photolysis laser beam along the quartz tube, and on the Cl_2/CH_3OD ratio. An example of such dependence is shown in Fig. 3. The signals are normalized to the CH_2OD^+ intensity, obtained by 1+1 REMPI at ~244 nm via the origin band of the $3p_z\leftarrow 1\,^2A''$ transition. The closer the position of the Cl_2 photolysis beam along the quartz tube was to the aperture of the pulsed valve, the larger the signal at the low-energy region became. Clearly, when Cl production happens upstream along the quartz tube, the collision time between Cl and the reactants increases, enhancing the probability of secondary reactions. An enhancement of the low-energy peak was also observed when the relative concentration of Cl_2 was increased, again apparently due to the increased role of secondary reactions. Considering the variation of the low-energy D signal with experimental conditions, and its small intensity under conditions that discourage secondary reactions, we conclude that it probably arises from molecular products of secondary reactions, and not from photodissociation of CH_2OD.

By assuming a constant value of $\beta_{\text{eff}}\approx 0$ for the slow component and $\beta_{\text{eff}}=-0.7$ for the fast one, the relative contributions, $P_i(E_T)$, of the two sources can be deconvoluted based on the equations: $P(E_T)=P_{\text{I}}(E_T)+P_{\text{II}}(E_T)$, and $\beta_{\text{eff}}(E_T)=\chi_{\text{I}}(E_T)\beta_{eff_{\text{I}}}+\chi_{\text{II}}(E_T)\beta_{\text{eff}_{\text{II}}}$, where $\chi_i(E_T)=P_i(E_T)/P(E_T)$. In this way, the D signal deriving from the contamination is eliminated. The total c.m. translational energy distribution resulting only from the CH_2OD precursor is then calculated by using Eq. (2) and is shown in Fig. 4.

The negative β_{eff} value of -0.7 ± 0.1 is consistent with the $3s\,^2A'\leftarrow 1\,^2A''$ transition moment $\boldsymbol{\mu}$ which is perpendicular to the plane of CH_2OD ($3s$). It also suggests that

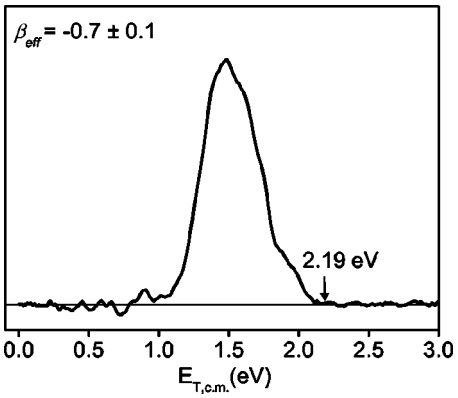

FIG. 4. Total c.m. translational energy distribution of the D channel from CH_2OD at 352.5 nm after eliminating the contribution from contaminations. The arrow indicates the value of $E_{T,\mathrm{c.m.}}^{\max}$ for $CH_2OD \rightarrow CH_2O\ (^1A_1) + D$ calculated using $D_0 = 1.32$ eV.

the dissociation from the excited state into products is faster than the rotational period of the parent. A large fraction of the available energy is partitioned into the translational degree of freedom with $\langle f_T \rangle = 0.69$. The nearly Gaussian shape of the distribution and the large value of $\langle f_T \rangle$ are consistent with the fast dissociation process. The arrow in Fig. 4 indicates the maximum allowed total c.m. translational energy of the products, $E_{T,\mathrm{c.m.}}^{\max} = 2.19$ eV, calculated for photolysis via channel I. For a parent rotational temperature of 10 K, $E_{\mathrm{int}}(CH_2OD) \cong 6\ \mathrm{cm}^{-1}$ and can be neglected in the calculation of $E_{T,\mathrm{c.m.}}^{\max}$. The calculated value of $E_{T,\mathrm{c.m.}}^{\max}$ is in good agreement with the experimentally observed maximum translational energy.

If isomerization to CH_2DO precedes dissociation (channel II), both H and D products should be observed at a ratio of 2:1; however, we detect only a small H signal, ~13 times smaller than D [see Fig. 5(a), solid line for H and closed circles for D]. The data shown are normalized by the laser power. In order to evaluate whether the small H signal is generated from CH_3OH isotopic contamination in the CH_3OD reactant, we carried out the same experiment with

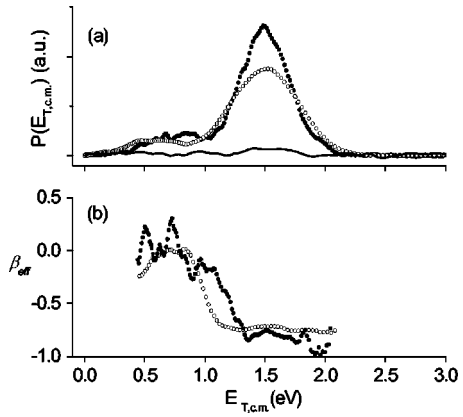

FIG. 5. (a) Products c.m. translational energy distributions obtained by detecting D (closed circles) and H (solid line) fragments from Cl_2/CH_3OD mixtures, and H fragments (open circles) from Cl_2/CH_3OH mixtures. (b) Products E_T-dependent anisotropy parameters obtained by detecting H from CH_2OH (open circles) and D from CH_2OD (closed circles).

CH_3OH precursor [Fig. 5(a), open symbols]. The total c.m. energy distribution of the H channel in the CH_3OH experiment was similar to that observed for D in the experiments with CH_3OD. The D and H E_T-dependent anisotropy parameters obtained from photodissociation of CH_2OD and CH_2OH, respectively, are shown in Fig. 5(b). The similarity of the total c.m. translational energy distributions and anisotropy parameters of the D and H channels supports our conclusions that the small H signal arises from CH_3OH contamination, and that O–D(H) fission is the main dissociation channel. Note also that the $E_{T,\mathrm{c.m.}}^{\max}$ value for CH_2OH is larger by 0.13 eV than $E_{T,\mathrm{c.m.}}^{\max}$ for CH_2OD, consistent with the energy difference between the dissociation thresholds. From this experiment, we conclude that the isomerization $CH_2OD \rightarrow CH_2DO$ is not favored. The absence of H products also excludes channels (IV) and (V) as major pathways.

In an attempt to evaluate the importance of channel (III), a search for CO ($v = 0$) signal was carried out by using (2+1) REMPI via the $B\ (^1\Sigma^+)$ state at 230.1 nm.[23] However, this experiment was hampered by a strong CO ($v = 0$) background signal from the probe laser alone. Coincidentally, the detection wavelength of CO (~230 nm) overlaps an absorption band of CH_2OD to the $3p_z$ Rydberg state,[24] and at this wavelength, the $CH_2O\ (^1A_1)$ product from CH_2OD photodissociation has sufficient internal energy to predissociate to CO ($v = 0,1$). The signal from this product overwhelms any other source of CO. We argue, however, that it is unlikely that channel (III) is competitive, because of the tight transition state and large barrier that are probably associated with H_2 elimination in the first dissociation step.[25]

The above-presented analysis provides considerable insight into the dissociation mechanism of CH_2OD. $CH_2OD \rightarrow CH_2O(^1A_1) + D(^2S_0)$ is the main open channel, and $\beta_{\mathrm{eff}} = -0.7 \pm 0.1$ is close to the limiting value for the perpendicular $1\ ^2A'(3s) \leftarrow 1\ ^2A''$ transition,[12] indicating rapid dissociation. This is consistent with the broad and featureless absorption spectrum in this wavelength region.[14] The high translational energy of most of the products indicates the existence of strong repulsive exit channel forces.

It has been shown before that the electronic wave function of the ground state of $CH_2OH(D)$ complies with Cs A'' symmetry (as a result of the shallowness of the CH_2 wag and O–H torsional potentials), while the *nuclear* equilibrium geometry of the radical calculated *ab initio* is nonplanar and belongs to the C_1 point group (A symmetry).[5] In A symmetry, the ground state correlates with $CH_2O(^1A_1) + D$ products, and the calculations performed by Saebo *et al.* found that this channel proceeds over a barrier of ~1.98 eV ($16\,000\ \mathrm{cm}^{-1}$).[9] Since electronic Rydberg states correlate diabatically with products in excited Rydberg states, the dissociation from the $3s$ state to channel (I) should involve crossing to the ground state PES.

Understanding the coupling between the $3s$ and the ground state is therefore essential for elucidating the dissociation mechanism, and indeed the calculations by Hoffman and Yarkony indicate that the excited state dissociation of CH_2OD is strongly affected by nonadiabatic transitions through conical intersections.[18] They find an efficient seam of conical intersections between the $3s$ and the ground states

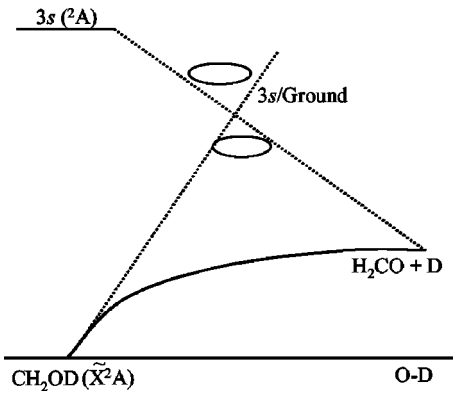

FIG. 6. Conical intersections between 3*s* and the ground state along the O–D coordinate, adapted from Ref. 18.

(see Fig. 6), with a low-energy (2.9 eV) crossing seam at an O–D distance of ~1.48 Å, i.e., extended by ~0.5 Å from the equilibrium distance in the ground state. This crossing region is reasonable, because at the ground state equilibrium geometry the two surfaces are widely separated and are not expected to intersect. In order to describe how the radical approaches the crossing seam from the 3*s* state, a calculation of the energy of this state is also performed along a gradient directed path originating on the 3*s* PES at the equilibrium geometry of the ground state. Until the gradient directed path reaches the 3*s*/ground seam of conical intersection, no local minimum is found.

The calculations support a mechanism involving a fast approach of the excited molecule to the intersection region. This conical intersection is thought to greatly promote radiationless transitions from 3*s* to the ground state. The 3*s*/ground state coupling transports the radical to a repulsive part of the ground state PES, where it dissociates to H_2CO $(1\,^1A_1)+D$. The excited radical does not have sufficient time to undergo intramolecular vibrational redistribution, or to form the bridged structure required for isomerization,[9] and dissociates directly on the repulsive region of the ground state with a large kinetic energy release. A similar mechanism has been suggested for the photodissociation of ethyl radical at 205.14 nm.[26]

To confirm the generality of the above-described findings, we carried out experiments at additional wavelengths. In the wavelength region 365–318 nm, similar D translational energy distributions and anisotropy parameters are observed as those at 352.5 nm. However, at wavelengths shorter than 318 nm, the H+HCOD channel deriving from direct C–H bond fission starts to contribute with gradually increasing participation. These results will be reported separately.

IV. CONCLUSIONS

The photodissociation dynamics of the 3*s* state of CH_2OD has been investigated, and D products angular and translational energy distributions are analyzed in detail following photodissociation at 352.5 nm. $CH_2OD \rightarrow CH_2O(^1A_1)+D$ is confirmed to be the main channel. The large fraction of the available energy deposited as translational energy, combined with the large negative value of β_{eff} (-0.7) indicate that O–D bond breaking is a fast process. The conical intersection calculations of Hoffman and Yarkony show that two steps are involved in this process: one begins on the 3*s* state and ends at the seam of a conical intersection where decay to the ground state occurs; the other describes the evolution of the system on the ground state from the crossing region to the final products. Both steps are fast and efficient and the final dissociation transpires on the repulsive region of the ground PES. Isomerization is not competitive with the fast dissociation on this state.

Several open questions still remain. The absence of a minimum on the 3*s* state, as obtained in the calculations of Hoffman and Yarkony, is puzzling considering its Rydberg character and the bound nature of the ground state of the ion. Also it is still unknown whether other repulsive states or other conical intersections participate in the photodissociation. We hope that our experimental studies will motivate a more complete characterization of the 3*s* PES, the seams of conical intersections connecting it to other surfaces, and other possible Rydberg–valence interactions.

ACKNOWLEDGMENTS

Support from the Chemical Sciences, Geosciences and Biosciences Division, Office of Basic Energy Sciences, U. S. Department of Energy and the Donors of the Petroleum Research Fund, administered by the American Chemical Society are gratefully acknowledged. We are indebted to David Yarkony for discussions regarding conical intersections in CH_2OH, and to Larry Harding for sending us unpublished results of calculations.

[1] B. J. Finlayson-Pitts and J. N. Pitts, Jr., *Chemistry of the Upper and Lower Atmosphere: Theory, Experiments, and Applications* (Academic, New York, 2000).
[2] J. J. Lin, J. Shu, Y. T. Lee, and X. Yang, J. Chem. Phys. **113**, 5287 (2000).
[3] J. Shu, J. J. Lin, Y. T. Lee, and X. Yang, J. Chem. Phys. **115**, 849 (2001).
[4] P. Pagsberg, J. Munk, A. Sillesen, and C. Anastasi, Chem. Phys. Lett. **146**, 375 (1988).
[5] R. D. Johnson and J. W. Hudgens, J. Phys. Chem. **100**, 19874 (1996).
[6] M. Ahmed, D. S. Peterka, and A. G. Suits, Phys. Chem. Chem. Phys. **2**, 861 (2000).
[7] S. Rudić, D. Ascenzi, and A. J. Orr-Ewing, Chem. Phys. Lett. **332**, 487 (2000); S. Rudić, C. Murray, D. Ascenzi, H. Anderson, J. N. Harvey, and A. J. Orr-Ewing, J. Chem. Phys. **117**, 5692 (2002).
[8] G. F. Adams, R. J. Bartlett, and G. D. Purvis, Chem. Phys. Lett. **87**, 311 (1982).
[9] S. Saebø, L. Radom, and H. F. Schaefer, J. Chem. Phys. **78**, 845 (1983).
[10] S. Dóbé, T. Bérces, T. Turányi, F. Márta, J. Grussdorf, F. Temps, and H. G. Wagner, J. Phys. Chem. **100**, 19864 (1996).
[11] C. Oehlers, H. G. Wagner, H. Ziemer, F. Temps, and S. Dóbé, J. Phys. Chem. A **104**, 10500 (2000).
[12] S. Rettrup, P. Pagsberg, and C. Anastasi, Chem. Phys. **122**, 45 (1988).
[13] P. J. Bruna and F. Grein, J. Phys. Chem. A **102**, 3141 (1998); **105**, 8599 (2001).
[14] L. Feng, X. Huang, and H. Reisler, J. Chem. Phys. **117**, 4820 (2002).
[15] V. Aristov, D. Conroy, and H. Reisler, Chem. Phys. Lett. **318**, 393 (2000).
[16] D. Conroy, V. Aristov, L. Feng, and H. Reisler, J. Phys. Chem. A **104**, 10288 (2000).
[17] D. Conroy, V. Aristov, L. Feng, A. Sanov, and H. Reisler, Acc. Chem. Res. **34**, 625 (2001).
[18] B. C. Hoffman and D. R. Yarkony, J. Chem. Phys. **116**, 8300 (2002).
[19] W. R. Simpson, A. J. Orrewing, T. P. Rakitzis, S. A. Kandel, and R. N. Zare, J. Chem. Phys. **103**, 7299 (1995).
[20] F. Fernandez-Alonso, B. D. Bean, and R. N. Zare, J. Chem. Phys. **111**, 1022 (1999).

[21] J. A. Syage, J. Chem. Phys. **105**, 1007 (1996).
[22] J. H. Wang, Y. T. Hsu, and K. Liu, J. Phys. Chem. A **101**, 6593 (1997).
[23] T. Droz-Georget, M. Zyrianov, H. Reisler, and D. W. Chandler, Chem. Phys. Lett. **276**, 316 (1997).
[24] L. Feng, A. Demyanenko, and H. Reisler, (unpublished).
[25] T. P. Marcy, R. R. Díaz, D. Heard, S. R. Leone, L. B. Harding, and S. J. Klippenstein, J. Phys. Chem. A **105**, 8361 (2001).
[26] Z. Y. Min, R. Quandt, and R. Bersohn, Chem. Phys. Lett. **296**, 372 (1998).